IEEE Access
Multidisciplinary | Rapid Review | Open Access Journal

Received November 22, 2019, accepted December 5, 2019, date of publication December 12, 2019,
date of current version December 23, 2019.

Digital Object Identifier 10.1109/ACCESS.2019.2959043

Tire State Stiffness Prediction for Improving Path Tracking Control During Emergency Collision Avoidance

SHAOSONG LI[1,2,3], GUODONG WANG[3], GUOYING CHEN[1], HONG CHEN[1,2], (Senior Member, IEEE), AND BANGCHENG ZHANG[3]

[1]State Key Laboratory of Automotive Simulation and Control, Jilin University, Changchun 130000, China
[2]Department of Control Science and Engineering, Jilin University, Changchun 130000, China
[3]School of Mechatronic Engineering, Changchun University of Technology, Changchun 130012, China

Corresponding author: Guoying Chen (chenguoying@jlu.edu.cn)

This work was supported in part by the Foundation of State Key Laboratory of Automotive Simulation and Control under Grant 20181101, in part by the National Natural Science Foundation of China under Grant 51905045, in part by the Key Technology on Major Program of Jilin Province under Grant 20170201005GX, and in part by the Postdoctoral Research Project of Jilin Province under Grant [2016]No.26.

ABSTRACT In this study, a model predictive path tracking control method based on the prediction of tire state stiffness is proposed to improve the path tracking performance at the limit of vehicle dynamics. Considering the influence of the nonlinear properties of tire force on vehicle dynamics, a nonlinear UniTire model is established, based on which a state stiffness 3D look-up table is designed to linearize the nonlinear tire model. The tire state stiffness in the prediction horizon is predicted by the vehicle motion model using the reference path information. A new linear time-varying path tracking control model in the prediction horizon is designed based on the predicted tire state stiffness. A nonlinear model predictive controller and a traditional linear time-varying model predictive controller are also designed and compared with the proposed method to verify the effectiveness and advantage of the latter. Results clearly show an improved control performance of the proposed method compared with the traditional method under the limit condition. Moreover, the calculation speed of the proposed method is faster than that of the nonlinear model predictive control method.

INDEX TERMS Path tracking, vehicle dynamics, model predictive control, UniTire model, state stiffness prediction.

I. INTRODUCTION

Human errors are identified as the primary reason for fatal driving accidents, with approximately 75 % of traffic accidents related to driver failures [1]. To further improve road traffic safety, the intelligent vehicle safety technology represented by advanced driver assistance systems (ADAS) has been paid increasing attention and development in recent years [2]. ADAS uses sensors to observe the environment, analyzes the risk level of the current driving environment on the basis of the perceived environmental information, and then decides whether an active intervention has to be performed to avoid or mitigate the accident [3]. Existing driver assistance systems primarily avoid collisions by emergency braking, but in some situations (e.g., sudden appearances of pedestrians and obstacles, high-speed driving conditions, etc.), collisions cannot be avoided even at full brake. Active steering intervention provides a new solution for emergency collision avoidance control in limit conditions. The advantage of steering control is that only a small lateral offset is required to avoid collisions. And the steering-based collision avoidance can be divided into shared steering control [4] and autonomous steering control. The main task of the former is to assist the driver to steering better and maintain the stability of the vehicle. The task of the latter is to plan a reasonable collision avoidance path and track the path well. Typical path planning methods for steering-based obstacle avoidance include clothoid and sigmoid functions [5], [6]. However, the path tracking control faces enormous challenges due to the nonlinearity of vehicle dynamics. The traditional control methods of path tracking control (robust control, fuzzy control, and sliding mode control [7]–[9]) simply depend on the current

The associate editor coordinating the review of this manuscript and approving it for publication was Bohui Wang.

environmental information and encounter difficulties in considering the dynamic constraints of vehicles [10]. Therefore, model predictive control (MPC) is increasingly being applied to the field of vehicle control [11]–[13]. The rolling optimization strategy of MPC can compensate, to a certain extent, for the uncertainties caused by model mismatch, distortion, and disturbance. Nevertheless, a large model error will seriously affects the system stability. In an emergency, the vehicle may be maneuvered to its handling limit to avoid collision. In these conditions, the accuracy of the model becomes critical to ensure vehicle stability.

Tire force is the primary nonlinear element for vehicle dynamics. Some studies in path tracking control often assume that the tire slip angle is small and the tire model is simplified to a linear tire model [14]–[16]. However, under a limit condition, the control effect of this method is limited. Therefore, using a nonlinear tire model to design the prediction model of the path tracking controller is necessary. However, the optimal solution of the nonlinear model predictive controller (NMPC) requires a complex numerical solution method, which will increase the computational burden of the controller and affect the real-time performance of the system. Therefore, designing a linear time-varying MPC (LTV-MPC) controller by linearizing the nonlinear model is a simple and effective method to balance the nonlinearity and real time of the system before the hardware processing capability is significantly improved. Previous studies [17]–[19] generally used the current vehicle state to linearize tire models and achieve a desired control effect. However, the tire force expression obtained by this linearization method remains constant in the prediction horizon. This method of tire force linearization becomes less accurate when the vehicle is near the dynamic limit. Therefore, Li *et al.* [20] proposed a vehicle stability control method based on LTV-MPC considering the changing trend of tire force in the prediction horizon, and the control effect is compared with the NMPC and traditional LTV-MPC methods under limit conditions. The results show that the control performance of the proposed method is obviously improved compared with the traditional method, and the real-time performance is much better than that of NMPC. In the field of path tracking control, Brown et al. [21] used the tire slip angle sequence solved by the previous step to successively linearize the tire force in the current prediction horizon and designed a path planning and tracking integrated MPC controller. The tracking control of various driving scenarios is realized on the actual vehicle. A similar approach was also used in [22]. This study introduces a control framework that combines path tracking, vehicle stability, and collision avoidance. Experimental results show that the controller can ensure the vehicle drives safely at the handling limit and avoid obstacles that suddenly appear in the turn. However, the above methods require the length of the control horizon to be equal to the prediction horizon, which makes the dimension of the control input to be solved increase, resulting in heavy computational burden on the solver. Moreover, these studies mainly focus on the low and medium speed conditions, and the control problems under the limit conditions such as high speed and low friction coefficient have not yet been discussed.

Therefore, this study proposes a new linear time-varying path tracking control method to improve the tracking performance under the limit conditions and reduce the computational burden of the controller. The method uses the reference path data to predict the tire state stiffness and then applies the predicted tire state stiffness to the linearization expression of the nonlinear tire model in the prediction horizon. To compare the control performance, the NMPC and the traditional LTV-MPC path tracking controller, in which the tire force is invariant in the prediction horizon, are also designed in this study. The effectiveness of the proposed method is verified by experiments on the Matlab and CarSim co-simulation platforms. For convenience of description, in this study, we record the traditional LTV-MPC as LTI-MPC and the proposed method as LTV-MPC.

The paper is organized as follows. Section II establishes the vehicle and tire model. Section III designs the controllers, including NMPC, LTI-MPC, and LTV-MPC. Section IV presents the results. Section V summarizes the conclusion and future work.

II. MODELING

A. VEHICLE MODEL

The vehicle model used in this study is shown in Fig. 1. In the figure, *xoy* is the vehicle body coordinate, the coordinate origin *o* is at the vehicle center of mass, *x* axis points to the forward direction of the vehicle, *y* axis is perpendicular to the *x* axis and points to the left side of the driver, and *XOY* is the geodetic coordinate. Table 1 presents the notations used in the vehicle model. To simplify the design of the controller, we make the following assumptions [20]:

- Ignore the influence of the steering system and directly take the front steering angle as the input.
- Ignore the effect of longitudinal dynamics, and it is considered that the longitudinal speed of the vehicle is constant and the road is flat.
- Ignore the effect of suspension.
- Ignore the effect of aerodynamic.

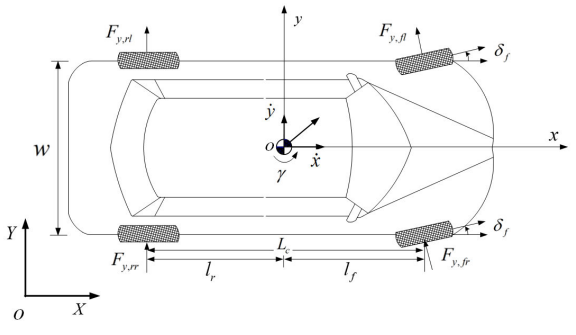

FIGURE 1. Vehicle model.

TABLE 1. Vehicle model notations.

Symbol	Description
$\dot{x}$	Longitudinal speed of vehicle
$\dot{y}$	Lateral speed of vehicle
γ	Vehicle yaw rate
δ_f	Front steering angle
F_y	Lateral tire force
$[fl, fr, rl, rr]$	Subscript fl, fr, rl and rr refer to the front left, front right, rear left, and rear right tires, respectively
l_f	Distance from the center of mass to the front axle
l_r	Distance from the center of mass to the rear axle
L_c	Distance between the front and rear axles
w	Distance between the left and right wheels

The yaw and lateral motion of a vehicle in geodetic coordinates can be expressed as

$$\begin{aligned} I_z\dot{\gamma} &= l_f F_{y,f} - l_r F_{y,r} \\ m\ddot{y} &= -m\dot{x}\gamma + F_{y,f} + F_{y,r} \\ \dot{\varphi} &= \gamma \\ \dot{Y} &= \dot{x}\sin\varphi + \dot{y}\cos\varphi \end{aligned} \tag{1}$$

where φ is the vehicle yaw angle in geodetic coordinates, m denotes the vehicle mass, and I_z represents the yaw moment of inertia, $F_{y,f}$ and $F_{y,r}$ are the lateral tire force at the front and rear axles, respectively, and $F_{y,f} = F_{y,fl} + F_{y,fr}$, $F_{y,r} = F_{y,rl} + F_{y,rr}$.

B. TIRE MODEL

Tire force is the main external force source for vehicle motion, which directly affects the vehicle stability at the handling limit. Therefore, a nonlinear tire model should be utilized to design the path tracking controller. The widely used tire models are Magic Formula, Fiala tire model, and UniTire model. UniTire model is proposed by Guo and Lu [23]. It is a nonlinear tire model for vehicle dynamic simulation and control, and it can describe tire properties accurately under complex conditions. Therefore, the UniTire model is used in this study.

The lateral forces given by the UniTire model are as follows [23]–[25]:

$$F_y = \bar{F}\frac{\phi_y}{\phi_n}\mu_y F_z. \tag{2}$$

$$\bar{F} = 1 - \exp\left(-\phi - E\phi^2 - \left(E^2 + \frac{1}{12}\right)\right)\phi^3. \tag{3}$$

$$E = \sqrt{\left(E_x\frac{\phi_x}{\phi}\right)^2 + \left(E_y\frac{\phi_y}{\phi}\right)^2}. \tag{4}$$

$$\phi_n = \sqrt{\left((\lambda\phi_x)^2 + \phi_y\right)^2}. \tag{5}$$

$$\phi = \sqrt{\left((\phi_x)^2 + \phi_y\right)^2}. \tag{6}$$

$$\lambda = \frac{1 + \frac{K_y}{K_x}\cdot\left(\frac{\phi}{\phi_c}\right)^\eta}{1 + \left(\frac{\phi}{\phi_c}\right)^\eta}. \tag{7}$$

TABLE 2. Unitire model notations.

Symbol	Description
F_y	Lateral tire force
$\bar{F}$	Dimensionless resultant force of tire
E	Curvature factor of combined slip resultant force
E_x	Curvature factor of longitudinal force
E_y	Curvature factor of lateral force
ϕ	Normalized combined slip ratio
ϕ_n	Modified normalized combined slip ratio
λ	Modification factor of the direction of resultant force
ϕ_x	Normalized longitudinal slip ratio
ϕ_y	Normalized lateral slip ratio
μ_x	Longitudinal friction coefficient
μ_y	Lateral friction coefficient
K_x	Longitudinal slip stiffness of the tire
K_y	Cornering stiffness of the tire
S_x	Longitudinal slip ratio
S_y	Lateral slip ratio
ω	Angular speed of wheel
V_x	Longitudinal relative sliding speed in the tire contact patch with respect to the road surface
V_y	Lateral relative sliding speeds in the tire contact patch with respect to the road surface
R_e	Effective rolling radius
κ	Tire longitudinal slip ratio in ISO tire coordinate
α	Tire lateral slip angle in ISO tire coordinate
F_z	Tire vertical load
F_{z0}	Maximum load on the tire
F_{zn}	Dimensionless tire vertical load

$$\phi_x = \frac{K_x S_x}{\mu_x F_z}; \quad \phi_y = \frac{K_y S_y}{\mu_y F_z}. \tag{8}$$

$$\left.\begin{aligned} \mu_x &= pu_1 + pu_2\cdot F_{zn} + pu_3\cdot F_{zn}^2 \\ \mu_y &= su_1 + su_2\cdot F_{zn} + su_3\cdot F_{zn}^2 \end{aligned}\right\}. \tag{9}$$

$$\left.\begin{aligned} E_x &= \frac{1}{\left(2 + pe_1{}^2\cdot exp\left(-F_{zn}\cdot pe_2\right)\right)} \\ E_y &= \frac{1}{\left(2 + se_1{}^2\cdot exp\left(-F_{zn}\cdot se_2\right)\right)} \end{aligned}\right\}. \tag{10}$$

$$\left.\begin{aligned} K_x &= \frac{F_z}{\left(pk_1 + pk_2\cdot F_{zn} + pk_3\cdot F_{zn}^2\right)} \\ K_y &= \frac{F_z}{\left(sk_1 + sk_2\cdot F_{zn} + sk_3\cdot F_{zn}^2\right)} \end{aligned}\right\}. \tag{11}$$

$$\left.\begin{aligned} S_x &= \frac{\omega R_e - V_x}{\omega R_e} = \frac{\kappa}{1+\kappa} \\ S_y &= \frac{-V_y}{\omega R_e} = -\left(1 - S_x\right)\cdot\tan\alpha \end{aligned}\right\}. \tag{12}$$

$$F_{zn} = \frac{F_z}{F_{z0}}. \tag{13}$$

Table 2 gives the notations used in the UniTire model, and Table 3 provides the parameters of the UniTire model. These parameters were obtained through our experiments and referenced to the study of Zhou [26].

The slip angle and vertical load for each tire are defined as

$$\begin{aligned} \alpha_{fl} &= \alpha_{fr} = \frac{\dot{y} + \gamma\cdot l_f}{\dot{x}} - \delta_f \\ \alpha_{rl} &= \alpha_{rr} = \frac{\dot{y} - \gamma\cdot l_r}{\dot{x}}, \end{aligned} \tag{14}$$

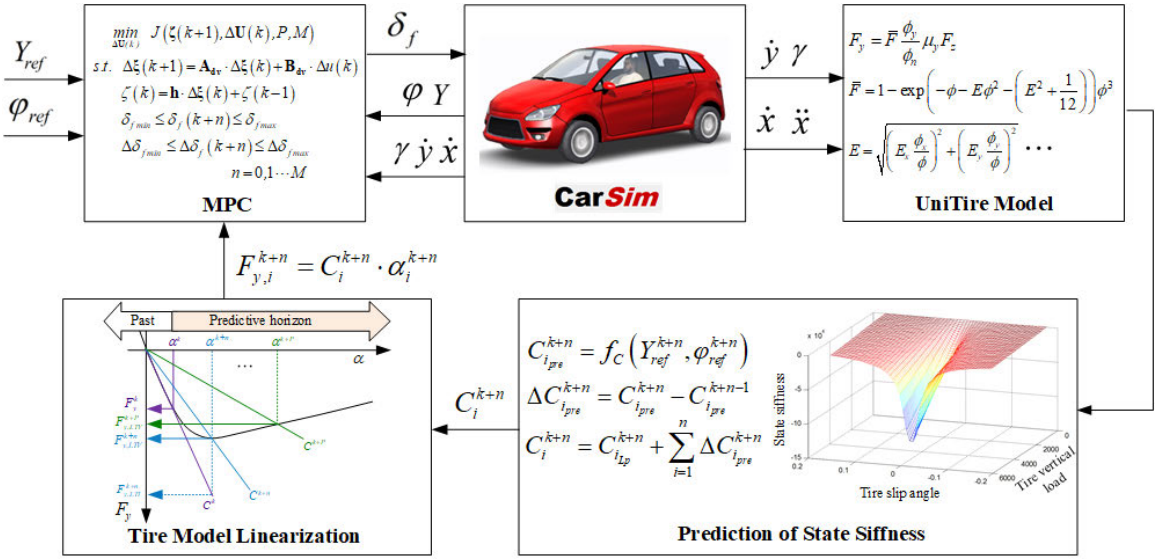

FIGURE 2. The overall structure of MPC path tracking controller.

TABLE 3. Unitire model parameters.

Parameters	Value	Parameters	Value
η	4	ϕ_c	1
pu_1	0.85	se_1	-2.08
pu_2	-0.298	se_2	9.37
pu_3	-0.298	pk_1	0.019
su_1	1.106	pk_2	-0.00000001
su_2	-0.36	pk_3	-0.00000001
su_3	0.051	sk_1	0.046
pe_1	-2.98	sk_2	0.008
pe_2	9.37	sk_3	0.006

$$
\begin{aligned}
F_{z,fl} &= \frac{mg}{2L_c}\left(l_r - \frac{h_g\ddot{x}}{g} - \frac{2l_r h_g \dot{x}\gamma}{gw}\right)\\
F_{z,fr} &= \frac{mg}{2L_c}\left(l_r - \frac{h_g\ddot{x}}{g} + \frac{2l_r h_g \dot{x}\gamma}{gw}\right)\\
F_{z,rl} &= \frac{mg}{2L_c}\left(l_f + \frac{h_g\ddot{x}}{g} - \frac{2l_r h_g \dot{x}\gamma}{gw}\right)\\
F_{z,rr} &= \frac{mg}{2L_c}\left(l_f + \frac{h_g\ddot{x}}{g} + \frac{2l_r h_g \dot{x}\gamma}{gw}\right),
\end{aligned}
\tag{15}
$$

where h_g is the height from the center of vehicle mass to the ground.

III. CONTROLLER DESIGN

Fig. 2 shows the overall structure of the controller, including tire model, tire state stiffness prediction, tire model linearization and MPC controller. In this study, it is considered that the collision avoidance path has been planned, and the design of path planning is not discussed here. In this section, the NMPC and LTI-MPC are first designed, and then the LTV-MPC based on tire state stiffness prediction proposed in this study is described in detail. In addition, the prediction method of state stiffness and linearization method of tire force based on state stiffness are introduced.

A. NMPC DESIGN

With (1)-(15), the prediction model of NMPC can be expressed as:

$$
\begin{aligned}
\dot{\xi} &= f_{u(t)}\left(\xi\left(t\right), u\left(t\right)\right)\\
\zeta &= h\left(\xi\left(t\right)\right),
\end{aligned}
\tag{16}
$$

where the state vector, control input and output are $\xi = [\dot{y}, \gamma, \varphi, Y]^T$, $u = \delta_f$ and $\zeta = [\varphi, Y]^T$ respectively, and the output map is given as

$$
h\left(\xi\right) = \begin{bmatrix} 0 & 0 & 1 & 0 \\ 0 & 0 & 0 & 1 \end{bmatrix} \cdot \xi
$$

Equation (16) is discretized by the fourth-order Runge-Kutta method, and the incremental discrete-time model is obtained as follows:

$$
\begin{aligned}
\xi\left(k+1\right) &= f_{\Delta u(t)}\left(\xi\left(k\right), \eta\left(\Delta u\left(k\right)\right)\right)\\
\zeta\left(k\right) &= h\left(\xi\left(k\right)\right)\\
\eta\left(\Delta u\left(k\right)\right) &= u\left(k\right) - u\left(k-1\right),
\end{aligned}
\tag{17}
$$

where the sampling time is $T_s = 0.01$.

According to MPC theory, the predictive output and control input sequence are obtained as follows:

$$
\zeta\left(k+1\right) = \left[\zeta\left(k+1\right)\cdots\zeta\left(k+P\right)\right]^T_{P\times 1}, \tag{18}
$$

$$
\Delta\mathbf{U}(k) = \left[\Delta u(k)\cdots\Delta u(k+M-1)\right]^T_{M\times 1}, \tag{19}
$$

where P is the prediction horizon and M is the control horizon. The subscripts $P \times 1$ and $M \times 1$ of the matrix represent the number of vectors or sub-matrices in the matrix and do not represent the dimensions of the matrix.

The reference output sequence for controller tracking is defined as follows:

$$
\mathbf{R}\left(k+1\right) = \left[\mathbf{r}\left(k+1\right)\cdots\mathbf{r}\left(k+P\right)\right]^T_{P\times 1}, \tag{20}
$$

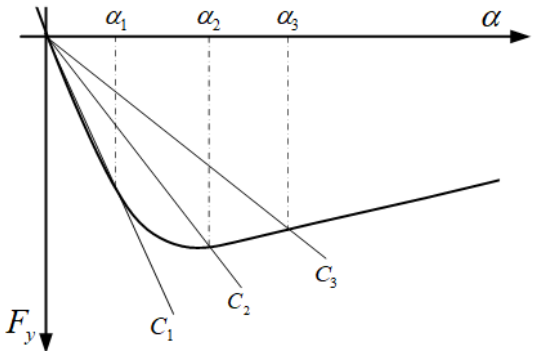

FIGURE 3. Lateral tire state stiffness.

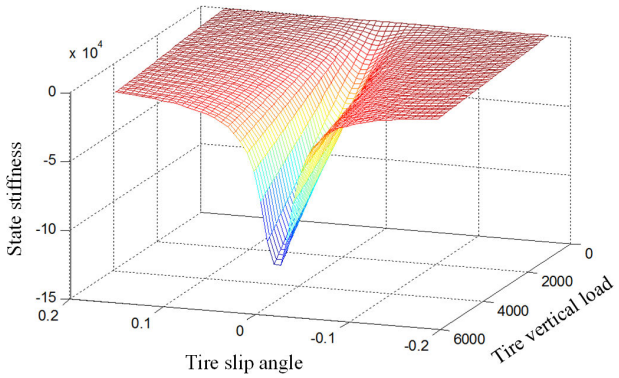

FIGURE 4. 3D map of state stiffness.

where $\mathbf{r} = [\varphi_{ref}, Y_{ref}]^T$, φ_{ref} and Y_{ref} are refer to the reference yaw angle and lateral position, respectively.

B. LTI-MPC DESIGN

1) TIRE MODEL LINEARIZATION

In previous studies [19], [20], the first-order Taylor expansion was used to linearize the tire force. However, this method introduces a residual lateral force [18], which increases the complexity of the model. Therefore, the state stiffness method is used to linearize the tire force in the current study. The concept of state stiffness is proposed by Guo [24], who defined lateral state stiffness as the ratio of lateral force to slip ratio at each lateral slip ratio, i.e., $K_{ys} = F_y/S_y$. A more detailed introduction can be found in [27].

According to the actual requirements of the control system design, in this study, lateral state stiffness is defined as the ratio of lateral force to tire slip angle at each tire slip angle, as shown in Fig. 3. The expression is as follows:

$$C = \frac{F_y}{\alpha}. \tag{21}$$

The linearized expressions of the lateral forces of each tire can then be obtained as follows:

$$F_{y,ij} = C_{ij} \cdot \alpha_{ij}, \tag{22}$$

where subscript $ij = fl, fr, rl$ and rr.

Therefore, for LTI-MPC, the tire force can be expressed as long as the lateral stiffness is obtained at the current tire slip angle and vertical load. In this study, a 3D look-up table of state stiffness is designed based on the nonlinear UniTire model. As shown in Fig. 4, the map of the state stiffness with the friction coefficient of 0.3 is given.

2) PREDICTION MODEL

Substituting (22) into (1), and assuming $\sin\varphi \approx \varphi$ and $\cos\varphi \approx 1$, can obtain the prediction model of LTI-MPC as follows:

$$m\ddot{y} = -m\dot{x}\gamma + C_f\left(\frac{\dot{y}+\gamma\cdot l_f}{\dot{x}} - \delta_f\right) + C_r\left(\frac{\dot{y}-\gamma\cdot l_r}{\dot{x}}\right)$$
$$I_z\dot{\gamma} = l_f C_f\left(\frac{\dot{y}+\gamma\cdot l_f}{\dot{x}} - \delta_f\right) - l_r C_r\left(\frac{\dot{y}-\gamma\cdot l_r}{\dot{x}}\right)$$
$$\dot{\varphi} = \gamma$$
$$\dot{Y} = \dot{x}\varphi + \dot{y}, \tag{23}$$

where C_f and C_r are the lateral state stiffness at the front and rear axles, respectively, and $C_f = C_{fl} + C_{fr}$, $C_r = C_{rl} + C_{rr}$.

Equation (23) is written as a standard state space equation as follows:

$$\dot{\xi} = \mathbf{A}\cdot\xi + \mathbf{B}\cdot u$$
$$\zeta = \mathbf{h}\cdot\xi, \tag{24}$$

where

$$\mathbf{A} = \begin{bmatrix} \frac{C_f + C_r}{m\dot{x}} & \frac{l_f C_f - l_r C_r}{m\dot{x}} - \dot{x} & 0 & 0 \\ \frac{l_f C_f - l_r C_r}{I_z\dot{x}} & \frac{l_f^2 C_f + l_r^2 C_r}{I_z\dot{x}} & 0 & 0 \\ 0 & 1 & 0 & 0 \\ 1 & 0 & \dot{x} & 0 \end{bmatrix},$$
$$\mathbf{B} = \left[-\frac{C_f}{m}, -\frac{l_f C_f}{I_z}, 0, 0\right]^T,$$
$$\mathbf{h} = \begin{bmatrix} 0 & 0 & 1 & 0 \\ 0 & 0 & 0 & 1 \end{bmatrix}.$$

Then, the incremental discrete model is obtained as follows:

$$\Delta\xi(k+1) = \mathbf{A_d}\cdot\Delta\xi(k) + \mathbf{B_d}\cdot\Delta u(k)$$
$$\zeta(k) = \mathbf{h}\cdot\Delta\xi(k) + \zeta(k-1). \tag{25}$$

3) PREDICTION EQUATION

On the basis of (25), the predicted output at time k can be expressed as

$$\zeta(k+1|k) = \mathbf{S}_\xi\cdot\Delta\xi(k) + \mathbf{I}\cdot\zeta(k) + \mathbf{S_u}\Delta\mathbf{U}(k), \tag{26}$$

where

$$\mathbf{S}_\xi = \begin{bmatrix} \mathbf{hA_d} \\ \vdots \\ \sum_{i=1}^{P}\mathbf{hA_d^i} \end{bmatrix}_{P\times 1}, \quad \mathbf{I} = \begin{bmatrix} \mathbf{I}_{n\zeta} \\ \vdots \\ \mathbf{I}_{n\zeta} \end{bmatrix}_{P\times 1},$$

$$\mathbf{S_u} = \begin{bmatrix} \mathbf{hB_d} & 0 & 0 \\ \vdots & \vdots & \vdots \\ \sum_{i=1}^{P} \mathbf{hA_d^{i-1}B_d} & \cdots & \sum_{i=1}^{P+M-1} \mathbf{hA_d^{i-1}B_d} \end{bmatrix}_{P\times M}.$$

C. LTV-MPC DESIGN

1) TIRE STATE STIFFNESS PREDICTION

Emergency scenarios may necessitate vehicle maneuvers up to their handling limits to avoid collisions [22]. In this condition, the tire force linearization method in LTI-MPC will produce a large error in the prediction horizon. As shown in Fig. 5, at time k, LTI-MPC linearizes the tire force at α^k, and as the prediction horizon rolls forward, the tire force error increasingly becomes larger. For example, at α^{k+n}, the tire force $F_{y,LTI}^{k+n}$ seriously deviates from the actual value of F_y^{k+n}.

Therefore, this study proposes a tire state stiffness prediction method to predict and linearize the tire force in the prediction horizon and solve the above problems. The expected effect is shown in Fig. 6.

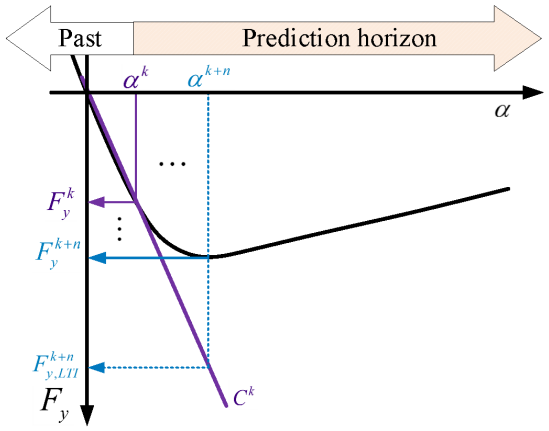

FIGURE 5. Tire force of LTI-MPC in the prediction horizon.

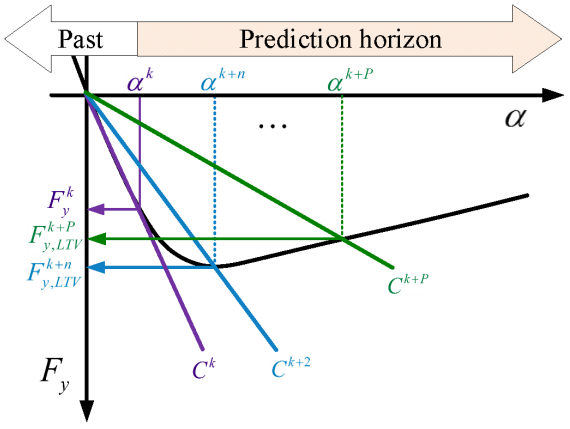

FIGURE 6. Tire force of LTV-MPC in the prediction horizon.

If the reference yaw angle and lateral position are known, then the expression for the tire force can be derived from (1) as follows:

$$\begin{aligned} \dot{\gamma} &= \kappa_{\mu,\dot{\gamma}} \ddot{\varphi}_{ref} \\ \ddot{y} &= \kappa_{\mu,\ddot{y}} \frac{\ddot{Y}_{ref}\cos\varphi_{ref} - \dot{Y}_{ref}\sin\varphi_{ref} + \dot{x}}{\cos^2\varphi_{ref}} \\ F_{y,f_{pre}} &= \kappa_{\mu,F} \cdot \frac{m\ddot{y}l_r + I_z\dot{\gamma} + m\dot{x}\gamma l_r}{(l_f + l_r)} \\ F_{y,r_{pre}} &= \kappa_{\mu,F} \cdot \frac{m\ddot{y}l_f - I_z\dot{\gamma} + m\dot{x}\gamma l_f}{(l_f + l_r)}, \end{aligned} \tag{27}$$

where $F_{y,f_{pre}}$ and $F_{y,f_{pre}}$ are the predicted tire force at the front and rear axles, respectively; φ_{ref} represents the reference yaw angle; Y_{ref} refers to the reference lateral position; and $\kappa_{\mu,\dot{\gamma}}$, $\kappa_{\mu,\ddot{y}}$, and $\kappa_{\mu,F}$ are adjustment factors that compensate for the influence of the friction coefficient. The values of $\kappa_{\mu,\dot{\gamma}}$ and $\kappa_{\mu,\ddot{y}}$ are the current friction coefficient and the values of $\kappa_{\mu,F}$ range from 0.5 to 0.8.

To avoid the tire force exceeding the adhesion limit, the tire force is constrained as follows:

$$\left|F_{y,i_{pre}}\right| \le \mu F_{z,i}, \tag{28}$$

where subscript $i = f, r$ refer to the front and rear axles.

Then the predicted tire slip angle can be obtained by the inverse tire model:

$$\alpha_{i_{pre}} = f_{tire}^{-1}\left(F_{y,i_{pre}}\right), \tag{29}$$

which is calculated offline and designed as a look-up table. Since the tire model is non-monotonic, the inverse tire model is represented by a piecewise function. As shown in Fig. 6, the tire model is divided into two parts, with the tire slip angle α_i^{k+n} as the boundary.

The predicted state stiffness can be obtained through the state stiffness look-up table. At time k, the future state stiffness can be expressed as

$$C_{i_{pre}}^{k+n} = f_C\left(Y_{ref}^{k+n}, \varphi_{ref}^{k+n}\right), \tag{30}$$

where $n = 1, 2, P$; $f_C(\cdot)$ represents (27)-(29)

Correspondingly, the increment of state stiffness can be expressed as

$$\Delta C_{i_{pre}}^{k+n} = C_{i_{pre}}^{k+n} - C_{i_{pre}}^{k+n-1}. \tag{31}$$

Finally, the state stiffness for linearization in the prediction horizon is as follows:

$$C_i^{k+n} = C_{i_{Lp}}^{k+n} + \sum_{i=1}^{n} \Delta C_{i_{pre}}^{k+n}, \tag{32}$$

where $C_{i_{Lp}}^{k+n}$ is the state stiffness from the look-up table based on the current tire slip angle and vertical load estimated by (14) and (15).

2) PREDICTION MODEL

Substituting (32) into (22) yields a linearized expression of the lateral force of the tire in the prediction horizon as follows:

$$F_{y,i}^{k+n} = C_i^{k+n} \cdot \alpha_i^{k+n}. \tag{33}$$

Next, the prediction model of LTV-MPC can be obtained by substituting (33) into (1) as follows:

$$\begin{aligned} \Delta\xi\,(k+1) &= \mathbf{A_{dv}} \cdot \Delta\xi\,(k) + \mathbf{B_{dv}} \cdot \Delta u\,(k) \\ \zeta\,(k) &= \mathbf{h} \cdot \Delta\xi\,(k) + \zeta\,(k-1)\,, \end{aligned} \tag{34}$$

where $\mathbf{A_{dv}}$ and $\mathbf{B_{dv}}$ are time-varying in the prediction horizon.

The predicted output of LTV-MPC can be obtained as:

$$\zeta(k+1|k) = \mathbf{S_{\xi v}} \cdot \Delta\xi(k) + \mathbf{I} \cdot \zeta(k) + \mathbf{S_{uv}}\Delta\mathbf{U}(k), \tag{35}$$

where,

$$\mathbf{S_{\xi v}} = \begin{bmatrix} \mathbf{h}\mathbf{A}_{\mathbf{dv}}^{k} \\ \mathbf{h}\mathbf{A}_{\mathbf{dv}}^{k} + \mathbf{h}\mathbf{A}_{\mathbf{dv}}^{k}\mathbf{A}_{\mathbf{dv}}^{k+1} \\ \vdots \\ \mathbf{h}\mathbf{A}_{\mathbf{dv}}^{k} + \cdots + \left(\mathbf{h}\mathbf{A}_{\mathbf{dv}}^{k}\mathbf{A}_{\mathbf{dv}}^{k+1} \cdots \mathbf{h}\mathbf{A}_{\mathbf{dv}}^{k}\mathbf{A}_{\mathbf{dv}}^{k+P}\right) \end{bmatrix}_{P\times 1},$$

$$\mathbf{S_{uv}} = [\mathbf{S_{uv1}}\,, \mathbf{S_{uv2}}, \cdots, \mathbf{S_{uv}}M\,],$$

$$\mathbf{S_{uv1}} = \begin{bmatrix} \mathbf{h}\mathbf{B}_{\mathbf{dv}}^{k} \\ \mathbf{h}\mathbf{B}_{\mathbf{dv}}^{k} + \mathbf{h}\mathbf{A}_{\mathbf{dv}}^{k}\mathbf{B}_{\mathbf{dv}}^{k} \\ \vdots \\ \mathbf{h}\mathbf{B}_{\mathbf{dv}}^{k} + \cdots + \left(\mathbf{h}\mathbf{A}_{\mathbf{dv}}^{k} \cdots \mathbf{A}_{\mathbf{dv}}^{k+P-1}\mathbf{B}_{\mathbf{dv}}^{k}\right) \end{bmatrix}_{P\times 1},$$

$$\mathbf{S_{uv2}} = \begin{bmatrix} 0 \\ \mathbf{h}\mathbf{B}_{\mathbf{dv}}^{k+1} \\ \vdots \\ \mathbf{h}\mathbf{B}_{\mathbf{dv}}^{k+1} + \cdots + \left(\mathbf{h}\mathbf{A}_{\mathbf{dv}}^{k+1} \cdots \mathbf{A}_{\mathbf{dv}}^{k+P-2}\mathbf{B}_{\mathbf{dv}}^{k+1}\right) \end{bmatrix}_{P\times 1},$$

$$\mathbf{S_{uv}}M = \begin{bmatrix} 0 \\ 0 \\ \vdots \\ \mathbf{h}\mathbf{B}_{\mathbf{dv}}^{k+M} + \cdots + \left(\mathbf{h}\mathbf{A}_{\mathbf{dv}}^{k+1} \cdots \mathbf{A}_{\mathbf{dv}}^{k+P-M}\mathbf{B}_{\mathbf{dv}}^{k+M}\right) \end{bmatrix}_{P\times 1}.$$

D. COST FUNCTION DESIGN AND OPTIMIZATION PROBLEM SOLVING

The control objectives of this study are to 1) track the reference lateral position and yaw angle and 2) keep the steering input smooth. Therefore, the cost function is designed based on a weighted combination of the error of lateral position and yaw angle, and control input rate:

$$\begin{aligned} J &= \left\|\Gamma_\zeta\left(\zeta\,(k+1) - \mathbf{R}\,(k+1)\right)\right\|^2 + \left\|\Gamma_u \Delta\mathbf{U}\,(k)\right\|^2 \\ &= \sum_{n=1}^{P}\left[\left(\varphi\,(k+n|k) - \varphi_{ref}\,(k+n)\right)^2 \cdot \tau_\varphi\right] \\ &\quad + \sum_{n=1}^{P}\left[\left(Y\,(k+n|k) - Y_{ref}\,(k+n)\right)^2 \cdot \tau_y\right] \\ &\quad + \sum_{n=1}^{M}\left[\left(\Delta\delta_f(k+n-1)^2\right) \cdot \tau_u\right], \end{aligned} \tag{36}$$

where $\Gamma_\zeta = diag\left(\left[\tau_\varphi, \tau_y\right]^T\right)_{P\times P}$, $\Gamma_u = diag(\tau_u)_{M\times M}$; τ_y, τ_φ, and τ_u are the weighting factors for tracking the lateral position, yaw angle, and rate of control input, respectively.

To avoid saturation of the mechanical system, the steering angle and steering range rate should be constrained:

$$\begin{aligned} -\delta_{f\max} \le \delta_f \le \delta_{f\max} \\ -\Delta\delta_{f\max} \le \Delta\delta_f \le \Delta\delta_{f\max}. \end{aligned} \tag{37}$$

The MPC based optimization problem for path tracking control can be defined as follows:

$$\begin{aligned} &\min_{\Delta U(k)} J\left(\zeta\,(k+1)\,, \Delta U\,(k)\,, P, M\right) \\ &s.t.\ \Delta\xi\,(k+1) = A_{dv} \cdot \Delta\xi\,(k) + B_{dv} \cdot \Delta u\,(k) \\ &\quad \zeta\,(k) = h \cdot \Delta\xi\,(k) + \zeta\,(k-1) \\ &\quad \delta_{f\min} \le \delta_f\,(k+n) \le \delta_{f\max} \\ &\quad \Delta\delta_{f\min} \le \Delta\delta_f\,(k+n) \le \Delta\delta_{f\max} \\ &\quad\quad n = 0, 1\cdots M. \end{aligned} \tag{38}$$

For NMPC, the nonlinear optimization problem is solved by the "Fmincon" function provided by the MATLAB optimization toolbox, and the sequence quadratic program algorithm is selected.

For LTI-MPC and LTV-MPC, the above constrained optimization problems are transformed into quadratic programming (QP):

$$\begin{aligned} &\min_{\mathbf{x}} \mathbf{x}^T\mathbf{H}\mathbf{x} - \mathbf{g}^T\mathbf{x} \\ &\tilde{\mathbf{C}}\mathbf{x} < \tilde{\mathbf{b}}, \end{aligned} \tag{39}$$

where $\mathbf{x} = \Delta\mathbf{U}(k)$, $\mathbf{H}$ is the Hessian matrix, $\mathbf{g}$ is the gradient vector, and $\tilde{\mathbf{C}}$ and $\tilde{\mathbf{b}}$ are the constraint matrices, defined as follows:

$$\begin{aligned} \mathbf{H} &= 2\left(\mathbf{S}_\mathbf{u}^T\Gamma_\zeta^T\Gamma_\zeta\mathbf{S_u} + \Gamma_\mathbf{u}\Gamma_\mathbf{u}\right) \\ \mathbf{g} &= -2\mathbf{S}_\mathbf{u}^T\Gamma_\zeta^T\Gamma_\zeta\mathbf{E_P} \\ \mathbf{E_P} &= \mathbf{R}\,(k+1) - \mathbf{S}_\xi\Delta x\,(k) - \mathbf{I}\cdot\zeta\,(k) \\ \tilde{\mathbf{C}} &= [\mathbf{I}^T, -\mathbf{I}^T, \mathbf{L}^T, -\mathbf{L}^T]^T \\ \mathbf{L} &= \begin{bmatrix} \mathbf{I}_{n_u} & 0 & 0 \\ \vdots & \vdots & \vdots \\ \mathbf{I}_{n_u} & \cdots & \mathbf{I}_{n_u} \end{bmatrix}_{M\times M} \\ \tilde{\mathbf{b}} &= \begin{bmatrix} \Delta\mathbf{U}(k)_{\max} \\ -\Delta\mathbf{U}(k)_{\min} \\ \mathbf{U}_{\max}\,(k) - u\,(k-1)\times ones\,(M,1) \\ u\,(k-1)\times ones\,(M,1) - \mathbf{U}_{\min}\,(k) \end{bmatrix}_{4M\times 1} \end{aligned}$$

In this study, the interior point method is used to solve the aforementioned QP problem.

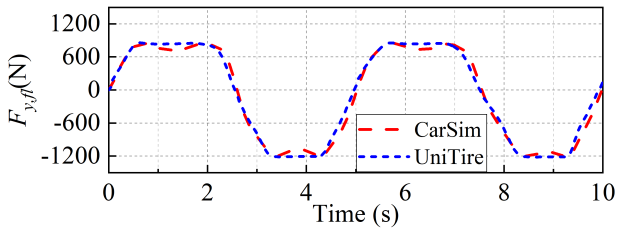

(a) Tire lateral force at the front left tire.

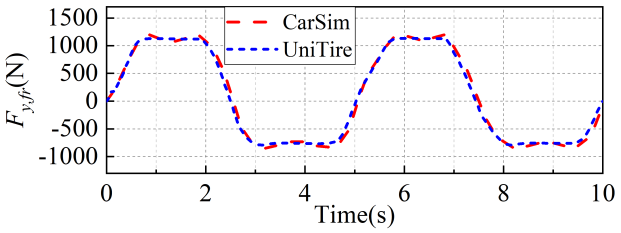

(b) Tire lateral force at the front right tire.

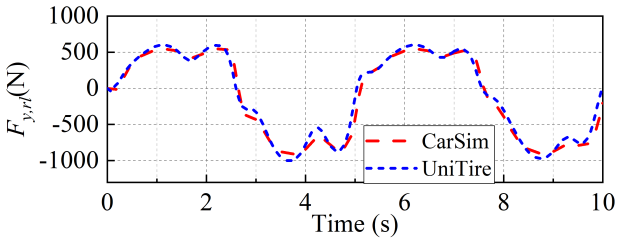

(c) Tire lateral force at the rear left tire.

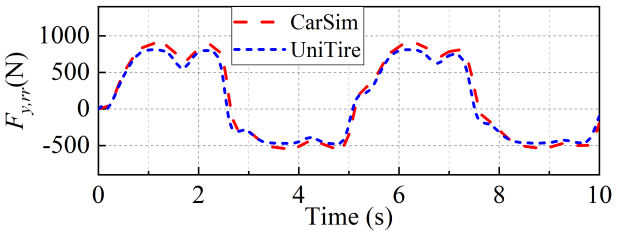

(d) Tire lateral force at the rear right tire.

FIGURE 7. **Comparison of tire force between UniTire model and CarSim.**

IV. SIMULATION RESULTS

The simulation experiments are based on MATLAB and the CarSim co-simulation environment. The section includes three parts: the first validates the tire model, the second validates the prediction method of state stiffness, and the third verifies the effectiveness of the proposed LTV-MPC path tracking controller through the lane change and double lane change tests.

A. TIRE MODEL VERIFICATION

For nonlinear MPC, the precision of tire model directly affects its control effect. For LTI-MPC and LTV-MPC, the precision of tire model affects the accuracy of linearization and the final control effect. Therefore, we match the tire model with CarSim.

Fig. 7 shows the tire force simulation results output by the UniTire model and CarSim with sine maneuver. The speed is 80 km/h, and the friction coefficient is 0.3.

The tire force of CarSim in Fig. (a)-(b) basically remains unchanged or slightly decreases at the crest and trough, while the tire force in Fig. (c)-(d) shows a significant decrease at the crest and trough. This finding indicates that the tire force is saturated under this condition. Fig. (a)-(d) reveals that even at this limit condition, the tire force of the UniTire model is almost the same as that of CarSim. This similarity means the established tire model is accurate enough to guarantee the accuracy of the tire model's linearization.

B. VERIFICATION OF STATE STIFFNESS PREDICTION

The comparison between actual and predicted values of state stiffness in the lane change maneuver is given in Fig. 8 to prove the feasibility and effectiveness of the proposed state stiffness prediction method. The speed is 80 km/h, and the friction coefficient is 0.3.

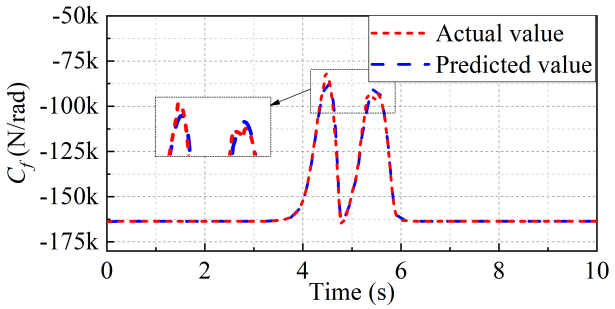

(a) Tire state stiffness at the front tires.

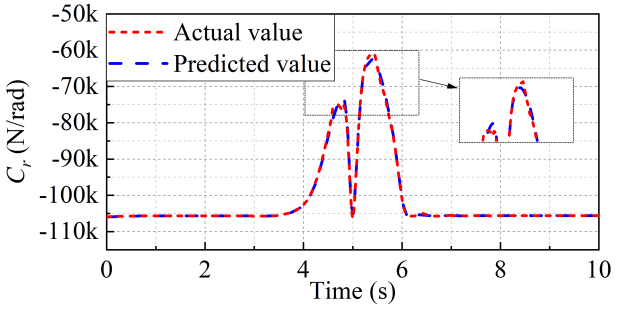

(b) Tire state stiffness at the rear tires.

FIGURE 8. **Comparison of tire state stiffness.**

Fig. 8(a) shows that the predicted value of the state stiffness of the front tire is slightly offset from the actual value at the peak around 4.5 s and 5.5 s, and the maximum deviation of 8929.05 N/rad occurs at 4.65 s. At other times, the predicted value of it is basically the same as the actual value. As can be seen in Fig. 8(b), the change in the state stiffness of the rear tire is similar to the front tire, and the state stiffness reach the peak at about 4.8 s and 5.2 s. The maximum deviation between the predicted value and the actual value is 3629.21 N/rad occurring at 4.79 s.

TABLE 4. Parameters of simulation vehicle and controller.

Vehicle Parameters	Value		
l_f	1.04 m		
l_r	1.56 m		
w	1.481 m		
m	1240 kg		
I_z	2031.4 kgm^2		
Controller Parameters	LTI-MPC	LTV-MPC	NMPC
T_s	0.01	0.01	0.01
P	50	50	50
M	1	1	1
$\delta_{f\max}$	10°	10°	10°
$\Delta\delta_{f\max}$	0.17°	0.17°	0.17°
$\tau_{\varphi,80}$	800	800	100
$\tau_{y,80}$	270	270	100
$\tau_{u,80}$	1130	1130	100
$\tau_{\varphi,110}$	1000	1000	800
$\tau_{y,110}$	100	100	100
$\tau_{u,110}$	8110	8110	4500

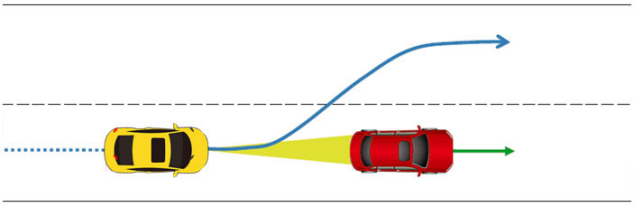

FIGURE 9. Scenario of lane change to avoid collision.

Remark 1: The actual value of state stiffness is obtained by inputting the tire slip angle and vertical load calculated in real time by (14) and (15) into the state stiffness look-up table. The predicted value of state stiffness is obtained by (32).

Remark 2: Only the curve of first value of the state stiffness prediction sequence is drawn in the figure.

C. PATH TRACKING TEST

To verify the proposed method, the line change and double line change path tracking tests have performed in this section. The performance was compared and analyzed with the LTI-MPC and NMPC tracking controller to evaluate the effectiveness and feasibility of the proposed LTV-MPC tracking controller. It should be noted that the reference path for line change is designed based on sigmoid function [6], and the reference path for double line change test is derived from the built-in driver model of CarSim. Table 4 gives the main parameters of the simulation vehicle and controller.

1) LANE CHANGE TEST

In the test, the vehicle performs a lane change maneuver on a road with a friction coefficient of 0.3 at a speed of 80 km/h to avoid collision. The collision avoidance scenario is shown in Fig. 9.

Fig. 10 shows the trajectory of the vehicle. The capability of LTI-MPC, LTV-MPC and NMPC to control the vehicle to track the reference lateral position is exhibited. The lateral position of LTI-MPC- and LTV-MPC-controlled vehicles is

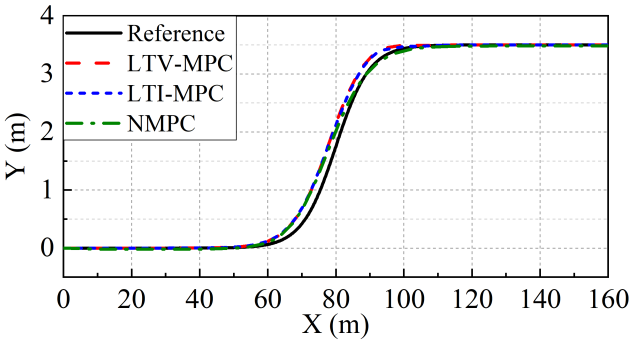

FIGURE 10. Vehicle trajectory.

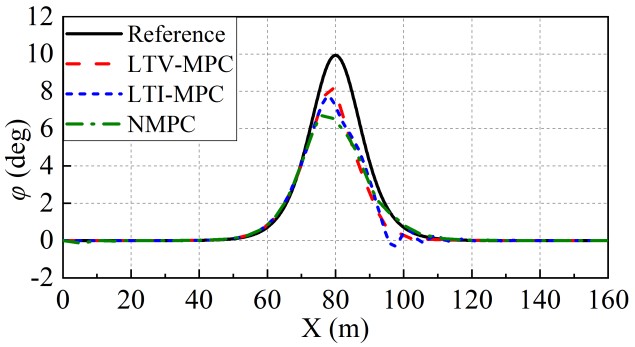

FIGURE 11. Yaw angle.

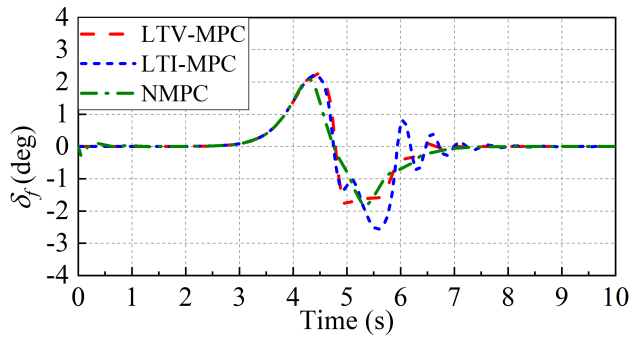

FIGURE 12. Front steering angle.

only slightly different from that of the NMPC-controlled vehicle from 80 m to 100 m. However, Fig. 11 shows that the yaw angle of the LTI-MPC-controlled vehicle fluctuates significantly when the vehicle is driving around 100 m. Overall, the path tracking effect of LTV-MPC is basically the same as that of NMPC, and they are better than that of LTI-MPC.

Remark 3: The phenomenon of phase advance in the results of lateral position and yaw angle is caused by the long prediction horizon. However, if the length of the prediction horizon is reduced, the controller will not be able to complete the tracking control.

Fig. 12 shows the front steering angle calculated by LTI-MPC, LTV-MPC, and NMPC controllers. Results show that the front steering angle calculated by NMPC is the smoothest,

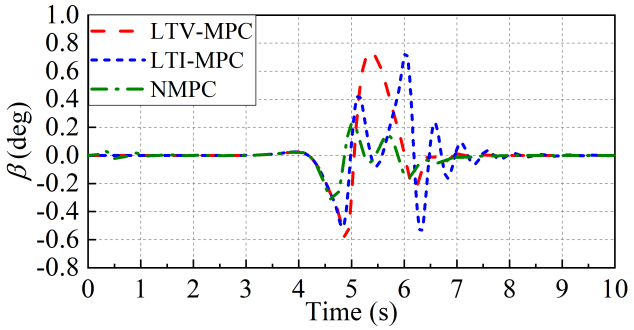

FIGURE 13. Vehicle sideslip angle.

and its maximum and minimum values are 2.0° and −1.9°, respectively. The maximum and minimum values of the front steering angle calculated by LTI-MPC reached 2.2° and −2.7° at 4.4 s and 5.6 s, respectively. Furthermore, a very serious jitter from 5 s to 7 s is also observed. The front steering angle calculated by LTV-MPC fluctuated slightly from 5 s to 7 s, with the maximum and minimum values of 2.2° and −1.8°, respectively. Due to the influence of the front angle, the vehicle sideslip angle has a similar response. Fig. 13 shows that the maximum and minimum values of the sideslip angles of LTI-MPC- and LTV-MPC-controlled vehicles are 0.73°, −0.57°, and 0.73°, −0.59°, respectively, which are approximately three times the sideslip angle of the NMPC-controlled vehicle. Fig. 13 presents that the stability of vehicle controlled by NMPC is the best, that controlled by LTI-MPC is the worst, and that controlled by LTV-MPC is between the two.

Fig. 14 shows the computation time for the LTI-MPC, LTV-MPC, and NMPC controllers. LTI-MPC consumes the least computation time, NMPC consumes the most computation time, and LTV-MPC saves about half of the computation time relative to NMPC. Results show that LTV-MPC has evident advantages over NMPC in computing speed, but further improvements are still needed compared with LTI-MPC.

2) DOUBLE LANE CHANGE TEST

The vehicle performs a double lane change maneuver on a road with a friction coefficient of 0.5 at a speed of 110 km/h to further verify the control effect of the proposed controller. The collision avoidance scenario is shown in Fig. 15.

Figs. 16 and 17 illustrate that LTI-MPC-controlled vehicles lose tracking at the limit condition. The loss of control occurs when the vehicle travels to about 150 m. The reason can be found in Fig. 18. From 4 s to 5 s, the front steering angle calculated by LTI-MPC fluctuates violently, and then the front steering angle rapidly increases and reaches the limit 10°. The front steering angle calculated by LTV-MPC also shows some fluctuations but remains to ensure proper tracking of the lateral position and yaw angle of the vehicle. Even the tracking effect of yaw angle of LTV-MPC from 90 m to 120 m is better than that of NMPC.

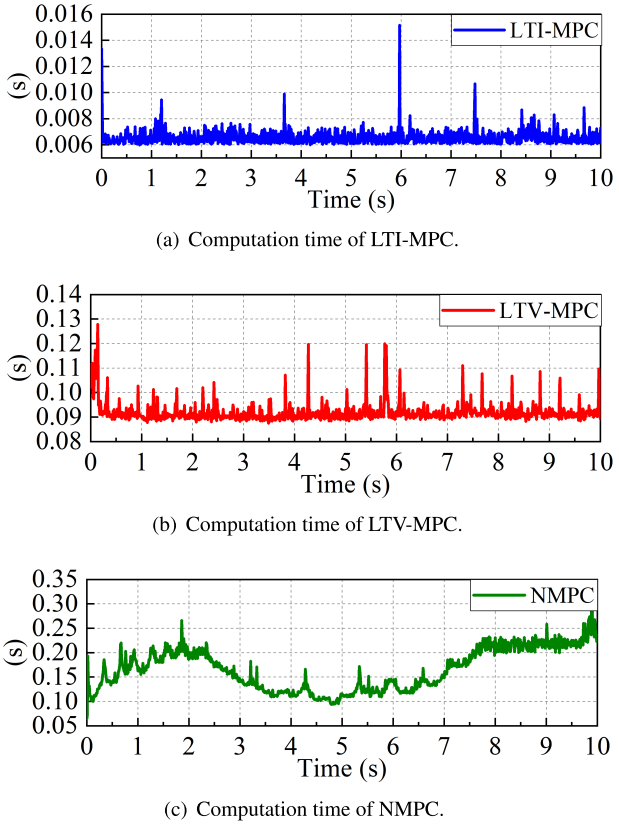

(a) Computation time of LTI-MPC.

(b) Computation time of LTV-MPC.

(c) Computation time of NMPC.

FIGURE 14. Computation time.

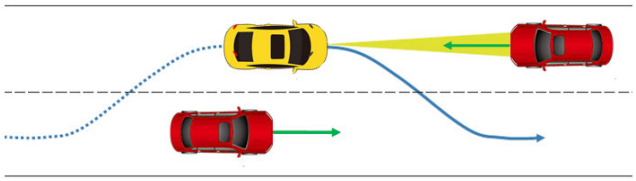

FIGURE 15. Scenario of double lane change to avoid collision.

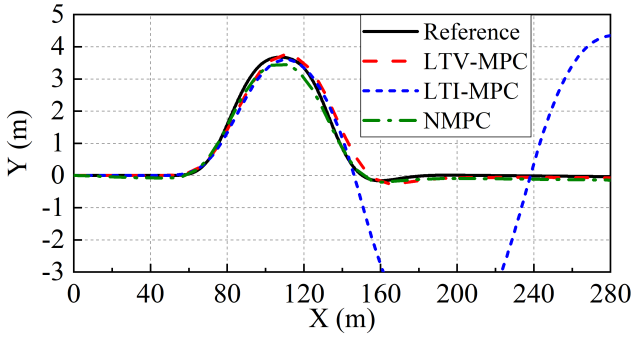

FIGURE 16. Vehicle trajectory.

Fig. 19 shows that the sideslip angle of the vehicle controlled by LTI-MPC becomes very large due to the loss of control of the vehicle. And the sideslip angle of the vehicle controlled by NMPC reaches 2.35° at 3.5 s, which is larger

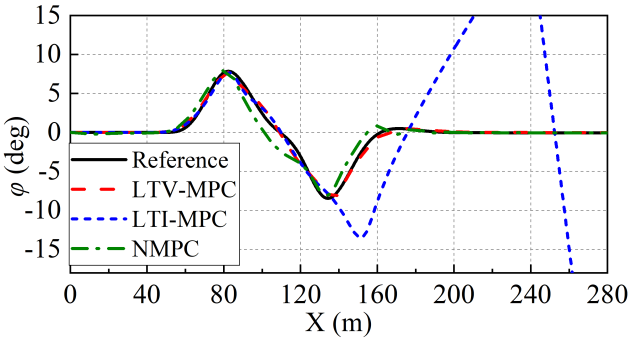

FIGURE 17. Yaw angle.

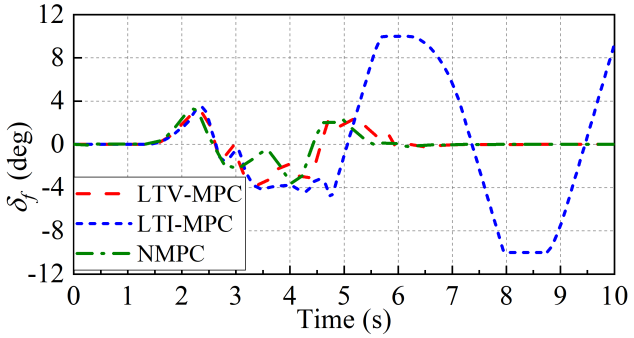

FIGURE 18. Front steering angle.

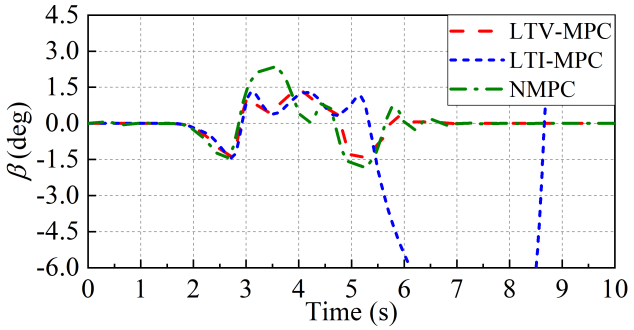

FIGURE 19. Vehicle sideslip angle.

than that of the other two. This phenomenon is caused by the increase in the front steering angle at around 3.5 s. The change of the sideslip angle of LTV-MPC controlled vehicle is the smallest, which indicates that the vehicle controlled by LTV-MPC has best stability.

The computation time shown in Fig. 20 has similar characteristics to the previous test result.

LTV-MPC can improve the control performance of the path tracking controller under limit conditions due to the precise linearization of the tire force. The control performance and calculation speed are improved compared with LTI-MPC and NMPC, respectively, and the desired control effect is achieved.

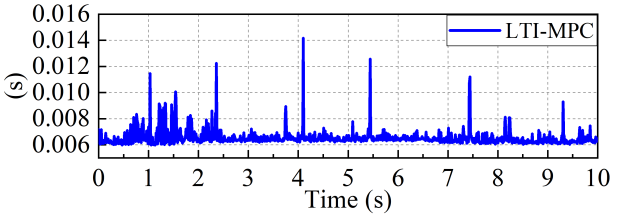

(a) Computation time of LTI-MPC.

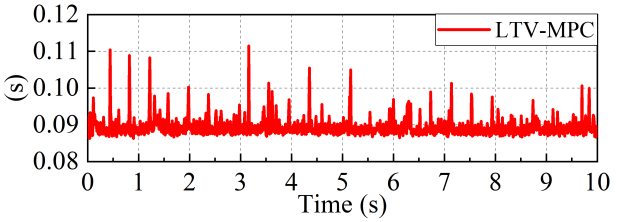

(b) Computation time of LTV-MPC.

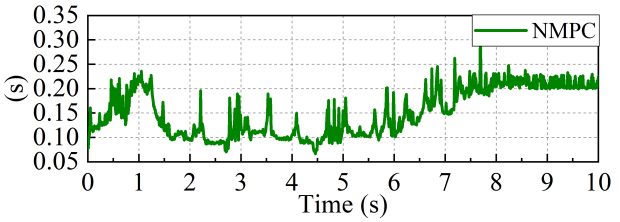

(c) Computation time of NMPC.

FIGURE 20. Computation time.

V. CONCLUSION

This study proposes a new LTV model predictive path tracking controller that considers the nonlinear trend of tire force in the prediction horizon. A state stiffness prediction method is designed to predict and linearize the tire model in the prediction horizon. Collision avoidance path tracking tests are carried out at different speeds on the wet road. Results show that the proposed path tracking controller can effectively improve vehicle path tracking ability and stability under the limit condition.

In this study, we find that improvements to vehicle's path tracking ability under the limit condition of only by steering are still limited. Therefore, in the next research, the path tracking performance and stability of the vehicle under the limit condition will be further improved by combining differential braking. The calculation speed of LTV-MPC needs to be further improved as well.

REFERENCES

[1] P. M. Salmon, M. A. Regan, and I. Johnston, "Human error and road transport: Phase two—A framework for an error tolerant road transport system," Monash Univ., Melbourne, VIC, Australia, Tech. Rep. 257, 2006.

[2] M. Flad, L. Fröhlich, and S. Hohmann, "Cooperative shared control driver assistance systems based on motion primitives and differential games," *IEEE Trans. Human-Mach. Syst.*, vol. 47, no. 5, pp. 711–722, Oct. 2017.

[3] A. E. D. Sc, B. V. Arem, A. Amditis, P. Lytrivis, E. Portouli, Z. Papp, B. D. Schutter, J. Ploeg, L. D. Baskar, and G. Naus, *Handbook of Intelligent Vehicles*. London, U.K.: Springer-Verlag, 2012.

[4] X. Na and D. J. Cole, "Game-theoretic modeling of the steering interaction between a human driver and a vehicle collision avoidance controller," *IEEE Trans. Human-Mach. Syst.*, vol. 45, no. 1, pp. 25–38, Feb. 2015.
[5] J. Funke and J. C. Gerdes, "Simple clothoid paths for autonomous vehicle lane changes at the limits of handling," in *Proc. ASME Dyn. Syst. Control Conf.*, 2013, pp. 1–10.
[6] C. Ackermann, J. Bechtloff, and R. Isermann, "Collision avoidance with combined braking and steering," in *Proc. 6th Int. Munich Chassis Symp.*, 2015, pp. 199–213.
[7] B. Mashadi, P. Ahmadizadeh, M. Majidi, and M. Mahmoodi-Kaleybar, "Integrated robust controller for vehicle path following," *Multibody Syst. Dyn.*, vol. 33, no. 2, pp. 207–228, 2015.
[8] C. Zhang, J. Hu, J. Qiu, W. Yang, H. Sun, and Q. Chen, "A novel fuzzy observer-based steering control approach for path tracking in autonomous vehicles," *IEEE Trans. Fuzzy Syst.*, vol. 27, no. 2, pp. 278–290, Feb. 2019.
[9] R. Wang, G. Yin, and X. Jin, "Robust adaptive sliding mode control for nonlinear four-wheel steering autonomous vehicles path tracking systems," in *Proc. Power Electron. Motion Control Conf.*, 2016, pp. 2999–3006.
[10] S. Chen, H. Guo, L. Feng, and C. Hong, "MPC-based path tracking controller design for autonomous ground vehicles," in *Proc. 36th Chin. Control Conf. (CCC)*, 2017, pp. 9584–9589.
[11] P. Falcone, F. Borrelli, J. Asgari, H. E. Tseng, and D. Hrovat, "Predictive active steering control for autonomous vehicle systems," *IEEE Trans. Control Syst. Technol.*, vol. 15, no. 3, pp. 566–580, May 2007.
[12] J. Ji, Z. Tang, M. Wu, and J. Fang, "Path planning and tracking for lane changing based on model predictive control," *China J. Highway Transp.*, vol. 31, no. 4, pp. 172–178, 2018.
[13] S. M. Erlien, S. Fujita, and J. C. Gerdes, "Shared steering control using safe envelopes for obstacle avoidance and vehicle stability," *IEEE Trans. Intell. Transp. Syst.*, vol. 17, no. 2, pp. 441–451, Feb. 2016.
[14] G. V. Raffo, G. K. Gomes, J. E. Normey-Rico, C. R. Kelber, and L. B. Becker, "A predictive controller for autonomous vehicle path tracking," *IEEE Trans. Intell. Transp. Syst.*, vol. 10, no. 1, pp. 92–102, Mar. 2009.
[15] Z. Wang, G. Li, H. Jiang, Q. Chen, and H. Zhang, "Collision-free navigation of autonomous vehicles using convex quadratic programming-based model predictive control," *IEEE/ASME Trans. Mechatronics*, vol. 23, no. 3, pp. 1103–1113, Jun. 2018.
[16] H. Guo, J. Liu, D. Cao, H. Chen, R. Yu, and C. Lv, "Dual-envelop-oriented moving horizon path tracking control for fully automated vehicles," *Mechatronics*, vol. 50, pp. 422–433, Apr. 2018.
[17] J. Chen, L. Li, and J. Song, "A study on vehicle stability control based on LTV-MPC," *Automot. Eng.*, vol. 38, pp. 308–317, Mar. 2016.
[18] M. Choi and S. B. Choi, "MPC for vehicle lateral stability via differential braking and active front steering considering practical aspects," in *Proc. Inst. Mech. Eng. D, J. Automobile Eng.*, vol. 230, no. 4, pp. 459–469, 2016.
[19] C. E. Beal and J. C. Gerdes, "Model predictive control for vehicle stabilization at the limits of handling," *IEEE Trans. Control Syst. Technol.*, vol. 21, no. 4, pp. 1258–1269, Jul. 2012.
[20] S. Li, G. Wang, B. Zhang, Z. Yu, and G. Cui, "Vehicle stability control based on model predictive control considering the changing trend of tire force over the prediction horizon," *IEEE Access*, vol. 7, pp. 6877–6888, 2019.
[21] M. Brown, J. Funke, S. Erlien, and J. C. Gerdes, "Safe driving envelopes for path tracking in autonomous vehicles," *Control Eng. Pract.*, vol. 61, pp. 307–316, Apr. 2017.
[22] J. Funke, M. Brown, S. M. Erlien, and J. C. Gerdes, "Collision avoidance and stabilization for autonomous vehicles in emergency scenarios," *IEEE Trans. Control Syst. Technol.*, vol. 25, no. 4, pp. 1204–1216, Jul. 2016.
[23] K. Guo and D. Lu, "Unitire: Unified tire model for vehicle dynamic simulation," *Vehicle Syst. Dyn.*, vol. 45, pp. 79–99, Jan. 2007.
[24] K. Guo, *Dyn Automobile Tyres*. Beijing, China: Science Press, 2018.
[25] K. Guo, "Unitire: Unified tire model," *J. Mech. Eng.*, vol. 52, no. 12, pp. 90–99, 2016.
[26] Y. Zhou, *Study Semi-empirical Non-steady Tire Model Combined-slip Condition*, Ph.D. dissertation, College Automot. Eng., Jilin Univ., Changchun, China, 2014.
[27] N. Xu and K. Guo, "Modeling combined braking and cornering forces based on pure slip measurements," *SAE Int. J. Commercial Vehicles*, vol. 5, pp. 470–482, Jan. 2012.

SHAOSONG LI received the Ph.D. degree in automotive engineering from Jilin University, Jilin, China, with a focus on vehicle dynamics and control.

He is currently a Teacher with the Changchun University of Technology. His current research interests include the application of control systems to vehicle dynamics to improve safety, stability, and performance of vehicles in conjunction with human drivers. He is a member of the Society of Automotive Engineers of China.

GUODONG WANG received the bachelor's degree in automotive engineering from the Huanghe Science and Technology College, Henan, China. He is currently pursuing the master's degree in automotive engineering with the Changchun University of Technology, Jilin, China.

His research interest includes the theory and technology of automotive safety and model predictive control.

GUOYING CHEN received the Ph.D. degree from Jilin University, Jilin, China, in 2012.

He is currently an Associate Professor with the State Key Laboratory of Automotive Simulation and Control, Jilin University. His research interest includes vehicle dynamics simulation and control.

HONG CHEN received the Ph.D. degree from the University of Stuttgart, Germany, in 1997.

She is currently a Professor with Jilin University, Jilin, China. Her research interests include model predictive control, nonlinear control, optimal and robust control, and automotive control.

BANGCHENG ZHANG received the B.Eng. and M.Eng. degrees from the Changchun University of Technology, Changchun, China, in 1995 and 2004, respectively, and the Ph.D. degree from Jilin University, China, in 2011.

He was an Academic Visitor with Tsinghua University, Beijing, China, in 2007. He is currently a Professor with the Changchun University of Technology. He has published about 20 articles. His research interests include mechatronics measurement technique and fault diagnosis.